Journal of Solid State Chemistry 182 (2009) 2068–2073

Contents lists available at ScienceDirect

Journal of Solid State Chemistry

journal homepage: www.elsevier.com/locate/jssc

Vibrational properties of the gallium monohydrides SrGaGeH, BaGaSiH, BaGaGeH, and BaGaSnH

Michael J. Evans [a], Myeong H. Lee [b], Gregory P. Holland [a], Luke L. Daemen [c], Otto F. Sankey [b], Ulrich Häussermann [a,*]

[a] Department of Chemistry and Biochemistry, Arizona State University, P.O. Box 871604, Tempe, AZ 85287-1604, USA
[b] Department of Physics, Arizona State University, P.O. Box 871504, Tempe, AZ 85287-1504, USA
[c] Lujan Neutron Scattering Center, Los Alamos National Laboratory, P.O. Box 1663, Los Alamos, NM 87545, USA

ARTICLE INFO

Article history:
Received 17 December 2008
Received in revised form
7 May 2009
Accepted 19 May 2009
Available online 27 May 2009

Keywords:
Metal hydrides
INS spectroscopy
Zintl phases

ABSTRACT

Vibrational properties of the gallium monohydrides SrGaGeH, BaGaSiH, BaGaGeH, and BaGaSnH (*Ae*Ga*Tt*H) have been investigated by means of inelastic neutron scattering (INS) and first principles calculations. The compounds contain separated Ga–H units being part of a two dimensional polyanionic layer, $[TtGaH]^{2-}$ (*Tt* = Si, Ge, Sn). The INS spectra show internal Ga–H bending and stretching modes at frequencies around 900 and 1200 cm^{-1}, respectively. While the stretching mode is virtually invariant with respect to the variable chemical environment of the Ga–H unit, the bending mode frequency varies and is highest for BaGaSiH and lowest for BaGaSnH. The stretching mode is a direct measure of the Ga–H bond strength, whereas the bending mode reflects indirectly the strength of alkaline earth metal–hydrogen interaction. Accordingly, the terminal Ga–H bond in solid state *Ae*Ga*Tt*H is distinct, but—compared to molecular gallium hydrides—very weak.

1. Introduction

Polyanionic hydrides are a family of mixed *s*- and *p*-block metal hydrides, which are obtained from the hydrogenation of Zintl phase precursors. The peculiar feature of these hydrides is the incorporation of H in polymeric anions composed of *p*-block atoms where it acts as a terminating ligand. This creates chemically new coordination environments for both metal and H atoms [1–4].

A fertile ground for precursors leading to polyanionic hydrides is provided by AlB_2-type variants among the ternary 9-electron systems *AeTrTt* (*Ae* = Ca, Sr, Ba; *Tr* = Al, Ga, In; *Tt* = Si, Ge, Sn) [4–7]. In the simple AlB_2 structure *Tr* and *Tt* atoms are randomly distributed on the majority site defining planar hexagon layers; variations may occur from *Tr*/*Tt* ordering and/or slight corrugations of hexagon layers [8]. The precursors *AeTrTt* are not electron precise (the optimum electron count for a polyanionic graphitic layer is 8 electrons per formula unit) and are metals. The silicides (*Tt* = Si) attracted interest for their superconducting properties, for which the partially occupied π^* band plays a decisive role [9,10]. Reaction with hydrogen leads to monohydrides *AeTrTt*H, which are electron precise Zintl phases with a narrow band gap. In these hydrides H is attached to the *Tr* atom and—compared to the AlB_2 type precursors—*TrTt* hexagon layers are substantially puckered [5,6].

Recently we reported on the crystal and electronic structure of a series of gallium monohydrides, SrGaGeH, BaGaSiH, BaGaGeH, BaGaSnH (*Ae*Ga*Tt*H), which contain isolated Ga–H entities in a flexible environment of group 14 (*Tt*) elements and alkaline earth metals [6]. Here we report on the vibrational properties of these compounds.

2. Experimental and computational details

The synthesis of the compounds SrGaGeH, BaGaSiH, BaGaGeH, and BaGaSnH is described in Ref. [6]. Solid-state ^2H magic angle spinning (MAS) NMR experiments were carried out at room temperature on a Varian VNMRS 400 MHz spectrometer equipped with a 3.2 mm triple resonance MAS probe operating at 61.4 MHz. Powders of BaGaSiD and BaGaGeD were packed in zirconia rotors and spun at a MAS frequency of 10 kHz. The ^2H signal transients were recorded with a single pulse $\pi/2$ (4 μs) and a 60 s recycle delay. ^2H chemical shifts were referenced indirectly by setting the ^2H resonance of D_2O to 4.8 ppm.

For INS spectroscopy the hydride samples (about 3 g) were loaded into an aluminum sample holder under a He atmosphere. The sample holder was subsequently sealed and mounted in a cryostat. The spectra of the two hydrides were measured at 10 K on the filter difference spectrometer (FDS) instrument at the Lujan

* Corresponding author.
E-mail address: Ulrich.Haussermann@asu.edu (U. Häussermann).

0022-4596/$ - see front matter © 2009 Elsevier Inc. All rights reserved.
doi:10.1016/j.jssc.2009.05.023

Center at Los Alamos National Laboratory. Data were treated by deconvolution of the instrumental resolution function. The two main algorithms used for FDS include a discrete, direct deconvolution [11] or the use of Bayesian methods (maximum entropy (ME)) [12]. Both methods are robust, with the first technique providing an energy resolution of the order of 4–5%, whereas maximum entropy is capable of reconstructing a vibrational spectrum with an energy resolution of the order of 2–3% and is useful to help resolve overlapping peaks or fainter features such as shoulders. However, the higher resolution achieved with ME comes sometimes at the price of spurious small intensity wiggles.

Theoretical calculations were performed using density functional theory with a planewave basis set and pseudopotential. The VASP [13] code was used for this purpose. We further used the generalized gradient approximation (GGA) of Perdew and Wang [14] to approximate the exchange-correlation energy. Ultra-soft pseudopotentials were used [15] to consider only the valence electrons in the calculations, and not the core electrons. For Sr and Ba semi-core *p* electrons were also included. The lattice parameters and the ionic positions were optimized for a fixed volume of the unit cell, and this process was repeated for several volumes. The equation of state was obtained and the optimized lattice constants were determined from the global minimum energy. For optimized cell parameters the internal coordinates of the unit cell were re-optimized to have zero-force. The Brillouin zone integration was performed over a $12 \times 12 \times 12$ Monkhorst–Pack grid [16]. The relaxed structural parameters are presented in Table 1.

The phonon vibrational modes were determined using a direct method [17] with supercells. In the direct method, one column of the dynamical matrix is obtained from the forces when a single atom is displaced by a finite displacement from its equilibrium position. The force is divided by the displacement to give a column of the force constant matrix. A $3a \times 3a \times 3c$ supercell was generated, and the position of all the atoms in the supercell was re-optimized using a $3 \times 3 \times 3$ k-point sampling until the forces converged to less than 0.1 meV/Å. Each atom in the supercell was displaced by 0.01 Å along each of the Cartesian directions, and the Hellmann–Feynman force on each atom was obtained. The number of atoms displaced was reduced by considering the symmetry. To remove cubic anharmonicity, the displacement of each atom was repeated in both the positive and negative directions, and the spring constants were averaged. We assumed a finite range of interaction (less than half the supercell dimensions) to obtain the wavevector dependent dynamical matrix. Normal mode frequency and eigenvectors were obtained by diagonalizing the wavevector dependent dynamical matrix to compute the INS spectra by the aCLIMAX program [18,19]. More details of phonon frequency calculations can be found in Ref. [20].

Table 1
Computationally relaxed structural parameters for *Ae*Ga*Tt*H (space group *P*3*m*1) compared with experimental parameters.

	SrGaGeH	BaGaSiH	BaGaGeH	BaGaSnH
a (Å)	4.2436	4.3162	4.3816	4.6022
exp.	4.2221(4)	4.2776(6)	4.3344(6)	4.559(1)
c (Å)	5.0238	5.3156	5.3290	5.4649
exp.	4.9691(6)	5.1948(9)	5.1895(9)	5.298(1)
Ga (1/3,2/3,*z*)	0.5575	0.5402	0.5490	0.5847
exp.	0.5585(2)	0.5267(8)	0.5432(1)	0.5509(3)
H (1/3,2/3,*z*)	0.9102	0.8734	0.8805	0.9076
exp.	0.9056(2)	0.8403(8)	0.8730(1)	0.8737(3)
Tt (2/3,1/3,*z*)	0.4379	0.4569	0.4497	0.4607
exp.	0.4402(2)	0.4395(10)	0.4437(1)	0.4424(3)

Exp. values refer to deuterides (Ref. [6]).

3. Results and discussion

3.1. Review of structural properties

The hydrides *Ae*Ga*Tt*H are obtained when exposing the 9-electron AlB_2-type phases *Ae*Ga*Tt* to a hydrogen atmosphere of 80 bar at temperatures between 275 and 425 °C. The trigonal structure of the *Ae*Ga*Tt*H compounds (SrAlSiH type, space group *P*3*m*1) displays slightly puckered hexagon layers in which Ga and *Tt* atoms are arranged strictly alternating (Fig. 1a). These layers are stacked on top of each other with the same orientation and sandwich *Ae* atoms. The structural parameters and interatomic distances from experiment (according to Ref. [6]) and computational relaxation (this work) are given in Tables 1 and 2, respectively.

H is exclusively attached to Ga and further coordinated by three *Ae* atoms (Fig. 1b). Overall, the different compositions *Ae*Ga*Tt*H produce only slight structural variations. The torsion angle (i.e. degree of puckering) decreases when going from SrGaGeH to BaGaGeH, and increases when going from *Tt* = Si to Sn within the BaGa*Tt*H series [6]. This correlates inversely with the *c*/*a* ratio. The Ga–H distance does not appear to be susceptible to the different chemical environments and is around 1.71 Å in the experimental crystal structure and around 1.77 Å in the computational relaxation. Although the Ga–H distance in *Ae*Ga*Tt*H formally corresponds to that of a terminal bond, it is relatively long compared to terminal Ga–H bond lengths in molecular species GaH_n ($n = 1, 2, 3$) or in the tetrahedral complex GaH_4^- occurring in $NaGaH_4$ [21,22]. The *Ae*–H distances correspond well to the shortest *Ae*–H distances in the binary salts AeH_2 with the cotunnite structure [23,24], with the exception of BaGaSnH where they appear substantially larger. The Ga–*Tt* distances are in the range typically observed for single bonded distances in Zintl phase polyanions. The calculated structural parameters agree reasonably

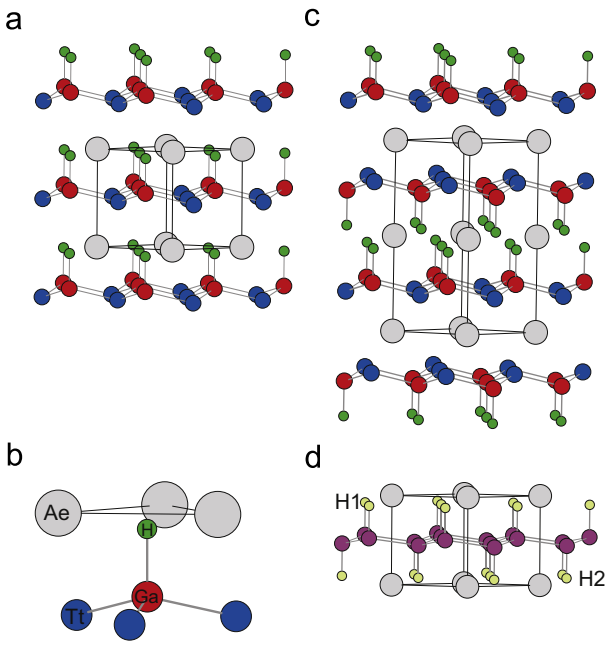

Fig. 1. (a) Crystal structure of the compounds *Ae*Ga*Tt*H (SrAlSiH-type). *Ae* (Sr, Ba), Ga, *Tt* (Si, Ge, Sn), and H atoms are denoted as grey, red, blue, and green circles, respectively. (b) Environment of the Ga–H unit in *Ae*Ga*Tt*H. (c) Variation of the SrAlSiH type structure based on two different hexagon layers with reversely arranged Ga and *Tt* atoms. (d) Average structure of disordered BaGaSiD. (Purple circles indicate mixed occupied Ga/Si positions and light green circles partially occupied D positions.) (For interpretation of the references to color in this figure legend, the reader is referred to the web version of this article.)

with the experimental ones. The *c* lattice parameter is notoriously overestimated which is especially noticeable for the Ba compounds (by about 3%). Larger deviations in the atomic position parameters occur for BaGaSnH.

Although the hydrogenation of AlB_2 type precursors induces only a minor structural change the reaction does not seem to follow a simple, topotactic-like, mechanism, which is indicated by the slow kinetics and rather high hydrogenation temperatures. This is plausible when considering the rearrangement of atoms within *Tr*/*Tt* disordered hexagon layers upon formation of ordered hydrides. For BaGaSi reaction with deuterium yields disordered BaGaSiD where the arrangement of Ga and *Tt* atoms within hexagon layers appears to be randomly reversed [6]. This "layer flip" is shown in Fig. 1c with an ordered model where the unit cell *c* axis is doubled. The refined model for BaGaSiD (Fig. 1d) corresponds to an average structure with two differently occupied *D* atom positions (40% and 60%, respectively) and a puckered hexagon layer with accordingly mixed occupied Ga/Si positions. This peculiarity was only observed for BaGaSiD [6].

Fig. 2 shows magic-angle spinning ^{2}H NMR spectra from powders of BaGaSiD and BaGaGeD. The *D* atom disorder by neutron diffraction in BaGaSiD is apparent from the very broad peak in the ^{2}H NMR spectrum. The ^{2}H NMR spectrum of BaGaGeD—which shows no crystallographic disorder in neutron powder diffraction—is more characteristic of a single site, although with a shoulder. This shoulder is also present in the ^{1}H NMR spectra of *Ae*Ga*Tt*H [6], which were the same samples employed for INS spectroscopy. The origin of the shoulder feature is not clear, but could be a consequence of inclusions of not hydrogenated precursor phase with sizes on the unit cell level in the hydride crystals. The H–H dipolar coupling as extracted from the DQ spinning sideband patterns of the primary and shoulder component of the ^{1}H resonance corresponds to a distance close to the *a* lattice parameter [6]. This is in agreement with this hypothesis, and precludes the presence of layer flip disorder where much shorter H–H distances (<3 Å) are expected.

Disorder represents a notorious feature for systems *Ae*Ga*Tt*H and *Ae*Ga*Tt*D. While neutron powder diffraction allows to detect D disorder and, thus, indirectly Ga/*Tt* disorder within the hexagon layers, a reliable direct refinement of Ga/*Tt* mixed occupancies for *Ae*Ga*Tt*H from X-ray powder diffraction data has proven impossible. Even in the case where atomic scattering factors are significantly different (Ga/Si, Ga/Sn) only a few reflections (e.g. 100 and 101) show intensity variations of more than 5%. Therefore hydride samples as employed for the INS study described here and deuteride samples used for the earlier described structural characterization could vary in terms of structural disorder. Both kinds of disorder, the one detectable by neutron powder diffraction (associated with D(Ga/*Tr*) disorder) and the one only detected by NMR (where we postulate precursor inclusions) seem to relate to the temperature applied in the hydrogenation. For more thermally stable aluminum hydride compounds where higher temperatures can be applied (e.g. SrAlSiH) disorder is not present [4].

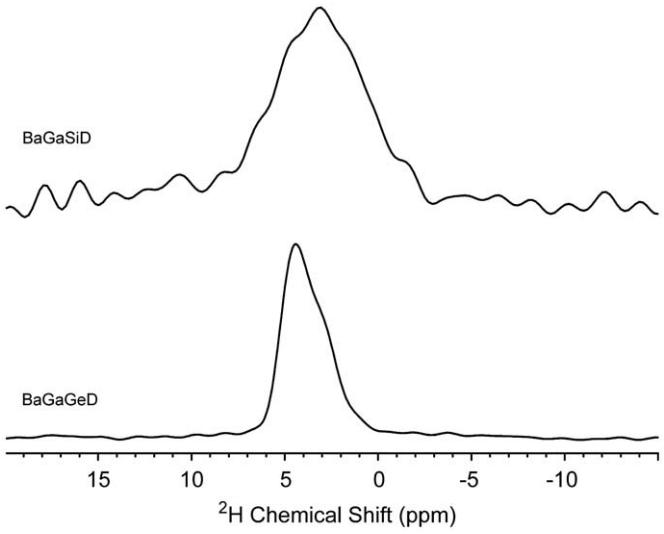

Fig. 2. ^{2}H MAS NMR spectra of BaGaSiD (top) and BaGaGeD (bottom). The poor signal-to-noise ratio in the BaGaSiD spectrum is the result of a limited amount of sample (about a fifth in volume of that for BaGaGeD).

3.2. INS spectroscopy

The INS spectra of *Ae*Ga*Tt*H are compiled in Fig. 3 for the range between 500 and 2700 cm^{-1}. The spectra are characterized by bands centered around 900 and 1200 cm^{-1} and associated overtones above 1500 cm^{-1}. These bands correspond to Ga–H bending and stretching modes (internal modes). The bending mode is degenerate. Vibrations stemming mainly from displacements of *Ae* and Ga atoms (external lattice modes) have much lower intensity and appear at lower frequencies (far below 500 cm^{-1}, not shown). In total, there are nine optic modes, which occur as three pairs (A_1+E): one pair of internal modes and two pairs of externals. The irreducible representations A_1 and E are according to point group C_{3v} and represent the main displacements along *z* ("out-of-plane") and *x*,*y* ("in-plane"), respectively.

The best resolved spectrum is that of BaGaSnH (Fig. 3d), showing the Ga–H bending mode at around 820 cm^{-1} and the stretching mode at around 1200 cm^{-1}. The 0–2 transitions (two quanta events) are the bending mode overtone, combination mode, and stretching mode overtone and appear at around 1640, 2000, and 2400 cm^{-1}, respectively. However, the resolution deteriorates at higher frequencies, and the latter overtone band is very broad. The experimental INS spectrum is compared to a calculated spectrum obtained by the program aCLIMAX [19] by using computed frequencies and displacements across the Brillouin zone. Originally, the calculated frequencies are underestimated by about 8%. When shifting the calculated frequencies of the bending mode to match the ones in the experimental spectrum and subsequently recalculating the INS spectrum, excellent agreement between calculated and experimental spectra is achieved. This scaling procedure is often performed to make frequencies from first principles calculations to coincide with experimental ones [18]. With agreement between experimental and calculated frequencies experimental spectra can be unambiguously evaluated.

The frequency of Ga–H stretching mode varies only slightly for the four different compositions *Ae*Ga*Tt*H. It is around 1190 cm^{-1} for the germanium compounds and reduces to around 1155 cm^{-1} for BaGaSiH. The bending mode, however, is more susceptible to compositional variations. The frequency increases within the BaGa*Tt*H series from 820 to 950 cm^{-1} and is around 905 cm^{-1} for SrGaGeH. In BaGaSiH, a shoulder feature appears to the low frequency side of the bending mode, and the reason for this is unclear. Structural disorder involving H could be an explanation but, as earlier discussed, ^{1}H NMR investigations do not support this.

In the *Ae*Ga*Tt*H compounds hydrogen is bonded terminally to Ga. The fundamental stretching mode is then a direct measure of the Ga–H bond strength. This mode is at very low wavenumbers compared to Ga–H stretching fundamentals in the molecular hydrides GaH, GaH_2, and GaH_3 which are $\approx$1650, $\approx$1800, and

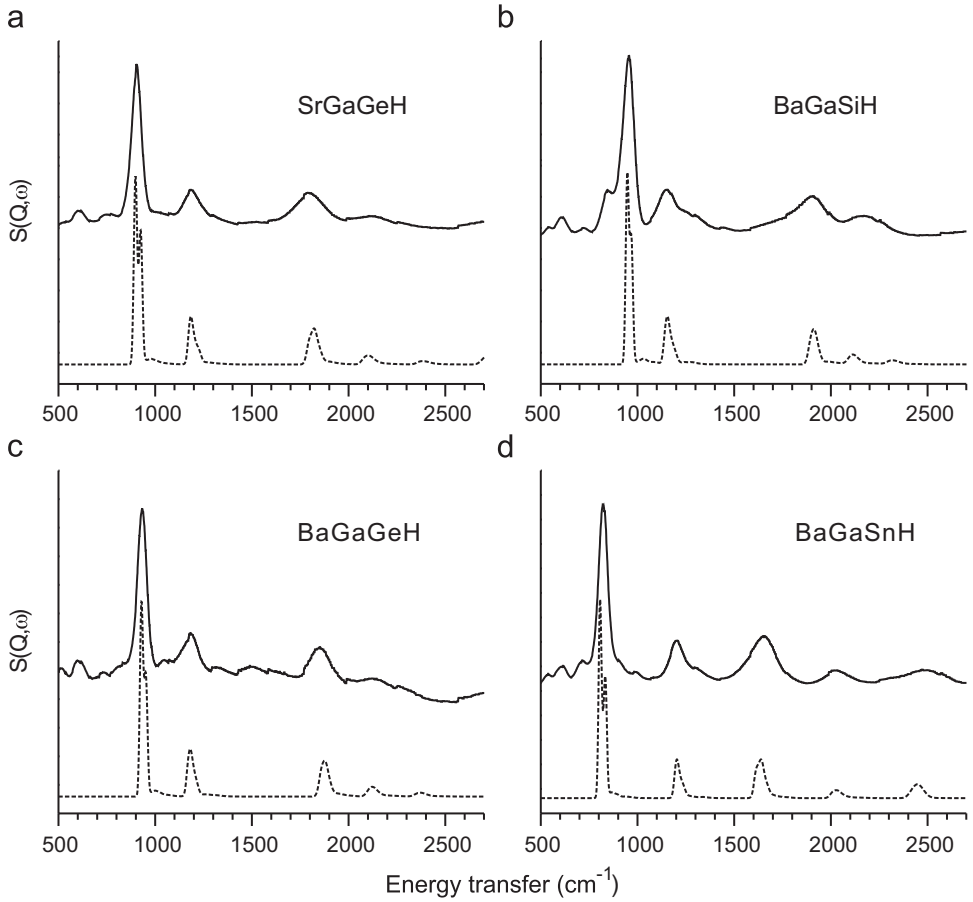

Fig. 3. Measured (solid line) and calculated (broken line) INS spectrum of SrGaGeH (a), BaGaSiH (b), BaGaGeH (c), and BaGaSnH (d). The calculated spectra are based on frequencies (scaled to match the experimental ones) and displacements obtained from first principles phonon calculations. In the spectra calculations overtones and combinations up to three quanta are included. Extra intensities in the experimental spectra (between 500 and 650 cm^{-1}) are spurious peaks introduced by the maximum entropy method used for deconvoluting the spectrometer data.

Table 2
Important interatomic distances (Å) in *Ae*Ga*Tt*H.

	SrGaGeH	BaGaSiH	BaGaGeH	BaGaSnH
Ga–H (× 1)	1.772	1.771	1.767	1.764
exp.	1.725(2)	1.726(7)	1.711(1)	1.708(3)
Ae–H (× 3)	2.491	2.581	2.609	2.705
exp.	2.482(1)	2.532(1)	2.587(1)	2.713(1)
Ga–*Tt* (× 3)	2.523	2.531	2.584	2.742
exp.	2.507(1)	2.512(1)	2.554(1)	2.691(1)
Ae–Ga (× 3)	3.308	3.490	3.490	3.495
exp.	3.279(1)	3.363(4)	3.446(1)	3.544(1)
Ae–*Tt* (× 3)	3.293	3.480	3.485	3.660
exp.	3.275(1)	3.485(3)	3.399(1)	3.521(1)

Exp. values refer to deuterides (Ref. [6]).

≈1900 cm^{-1}, respectively [21,25]. This implies that H is actually rather weakly bonded to Ga in *Ae*Ga*Tt*H. The bending modes—where H displaces toward *Ae* atoms—reflect indirectly the strength of *Ae*–H interactions and will stiffen (i.e. shift to higher frequencies) for stronger *Ae*–H interactions. Accordingly, those increase from *Tt* = Sn to Si within the BaGa*Tt*H series, roughly coinciding with the trend in the Ba–H distances (2.53, 2.59, and 2.71 Å for *Tt* = Si, Ge, and Sn, respectively; cf. Table 2).

3.3. Phonon dispersions

Fig. 4 shows the calculated phonon dispersions along special directions in the hexagonal Brillouin zone, and Table 3 lists the calculated frequencies at the Γ point. The degeneracy of modes at Γ—and other high-symmetry points—is removed at a general k point. The dispersion width of a mode relates to the broadness of the corresponding band in the INS spectrum.

The internal modes are weakly dispersed and their Γ point frequencies are slightly above 1100 cm^{-1} for the stretch and between 760 and 915 cm^{-1} for the bend. These frequencies are, as already mentioned, somewhat too low compared to the experimental INS spectra. Ga–H stretching and bending modes are separated widest for BaGaSnH, and become almost degenerate for BaGaSiH. Hydrogen is the most electronegative component in *Ae*Ga*Tt*H and it is reasonable to assume that it occurs hydridic (that is as H^-). At the same time the Zintl concept suggests that Ga atoms are considered as four-bonded. Therefore the Ga–H interaction is best described as a dative bond between H^- and nominally zero-charged Ga [$Ga \leftarrow H^{1-}$] [5]. This bond is weak–due to the strong, counteracting electrostatic *Ae*–H interaction–but distinct, as indicated by the rigid frequency of the stretching mode with respect to the various chemical environments in *Ae*Ga*Tt*H.

Turning to the external modes, the most interesting one is the in-plane Ga–*Tt* stretch (type *E*) mirroring the bond strength between such pairs of atoms. The calculated frequencies are around 190 cm^{-1} for Ga–Sn, around 225 cm^{-1} for Ga–Ge, and around 310 cm^{-1} for Ga–Si. Their ratios correspond quite precisely to the ratios of the expression $\sqrt{(1/m_{Ga}+1/m_{Tt})}$ for different *Tt*, which implies that Ga–*Tt* force constants are very similar. In BaGaGeH the Ga–Ge distance is elongated compared to SrGaGeH and the frequency of the in-plane stretching mode is lower by

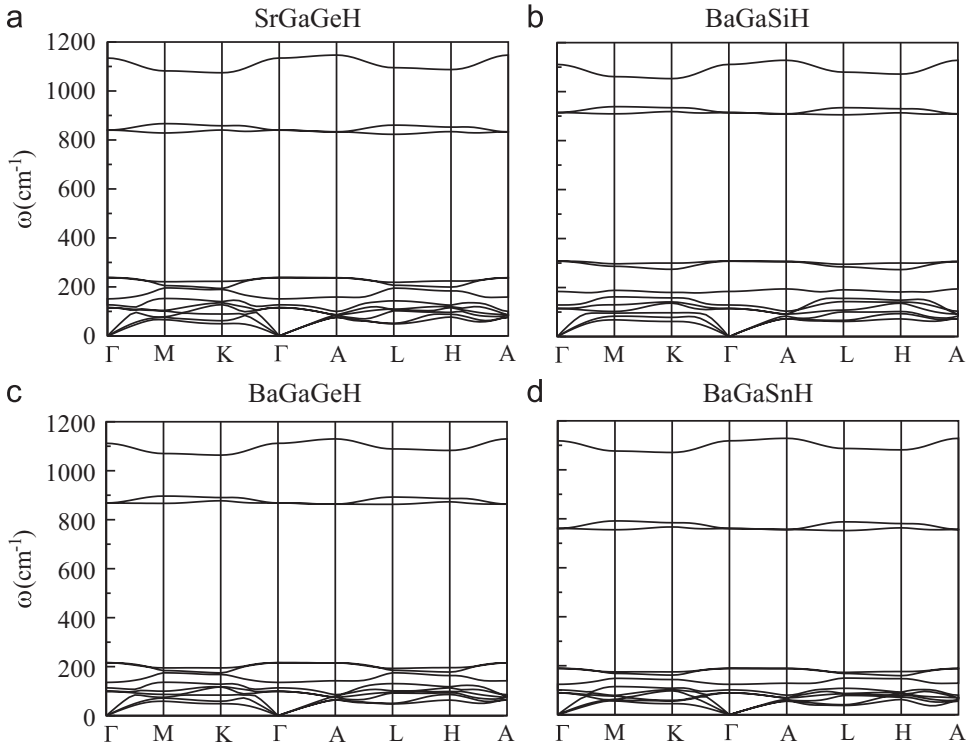

Fig. 4. Calculated phonon dispersion curves for SrGaGeH (a), BaGaSiH (b), BaGaGeH (c), and BaGaSnH (d) for the symmetry points of the Brillouin zone. The Cartesian *k*-points *A*, *L*, *M*, *Γ*, *H*, and *K* are $(2\pi/c)(0,0,1/2)$, $(2\pi/a)(1/2,\sqrt{3}/6,a/2c)$, $(2\pi/a)(1/2,\sqrt{3}/6,0)$, $(0,0,0)$, $(2\pi/a)(2/3,0,a/2c)$, $(2\pi/a)(2/3,0,0)$, respectively.

Table 3
Calculated phonon frequencies (in cm^{-1}) for optical modes at the *Γ* point (equilibrium lattice parameters).

Mode type	SrGaGeH	BaGaSiH	BaGaGeH	BaGaSnH
E (*Ae*)	115	114	99	89
A_1 (*Ae*)	127	129	113	101
A_1 (Ga–*Tt* out-of-plane)	151	184	136	124
E (Ga–*Tt* in-plane stretch)	238	308	216	189
E (Ga–H bend)	840	914	868	760
A_1 (Ga–H stretch)	1135	1111	1112	1119

All modes are both infrared and Raman active.

about 10%, which implies a slightly weaker Ga–Ge bond. To relate the strength of covalent Ga–Ge bonds in the polyanion of *Ae*GaGeH, we may simply compare with elemental germanium (similar "sp^3"-like bonding situation and similar atomic mass). Here the frequency of the optic phonon at $k = 0$ is 303 cm^{-1} [26]. Conclusively, although structures and bonding properties of polyanions in Zintl phases are likened to isoelectronic neutral arrangements the strength of element–element bonds in polyanions is much weaker.

4. Conclusions

Polyanionic hydrides offer new coordination environments for metal and H atoms. In particular, the isostructural compounds *Ae*Ga*Tt*H (*Ae* = Sr, Ba; *Tt* = Si, Ge, Sn) correspond to electron precise Zintl phases consisting of layered polyanions $[GaTtH]^{2-}$ with three-bonded $[Ga–H]^-$ and three-bonded, lone pair carrying Tt^- entities. The vibrational properties of *Ae*Ga*Tt*H were characterized by a combined inelastic neutron scattering and computational study. The Ga–H unit gives rise to bending and stretching modes at frequencies around 900 and 1200 cm^{-1}, respectively. The latter expresses the strength of the terminal Ga–H bond, which accordingly is very weak compared to molecular hydrides GaH_n ($n = 1, 2, 3$). Similar weak terminal Ga–H bonds have been observed earlier in the gallium dihydrides $SrGa_2H_2$ and $BaGa_2H_2$ which are isoelectronic to *Ae*Ga*Tt*H [27]. This phenomenon can be attributed to the effective coordination of H by *Ae* in the solid state polyanionic hydrides (strong electrostatic *Ae*–H interactions counteract the covalent Ga–H bond) and demonstrates the complex interplay of different metal–H interactions in multinary metal hydride systems.

Acknowledgments

This work has been supported by National Science Foundation Grant DMR-0638826 and has made use of the Manuel Lujan, Jr. Neutron Scattering Center at Los Alamos National Laboratory, which is funded by the Department of Energy's Office of Basic Energy Sciences. Los Alamos National Laboratory is operated by Los Alamos National Security, LLC, under DOE Contract DE-AC52-06NA25396. Additionally, the ASU Magnetic Resonance Research Center and partial support from DOE through Grant DE-FG02-05ER46235 are acknowledged.

References

[1] F. Gingl, T. Vogt, E. Akiba, J. Alloys Compd. 306 (2000) 127.
[2] T. Björling, D. Noréus, U. Häussermann, J. Am. Chem. Soc. 128 (2006) 817.
[3] M.H. Lee, O.F. Sankey, T. Björling, D. Moser, D. Noréus, S.F. Parker, U. Häussermann, Inorg. Chem. 46 (2007) 6987.
[4] T. Björling, D. Noréus, K. Jansson, M. Andersson, E. Leonova, M. Edén, U. Hålenius, U. Häussermann, Angew. Chem. Int. Ed. 44 (2005) 7269.

[5] M.H. Lee, T. Björling, T. Utsumi, D. Moser, D. Noréus, D. Bull, B. Hauback, O.F. Sankey, U. Häussermann, Phys. Rev. B 78 (2008) 195209.
[6] M.J. Evans, G.P. Holland, J.F. Garcia-Garcia, U. Häussermann, J. Am. Chem. Soc. 130 (2008) 12139.
[7] U. Häussermann, Z. Kristallogr. 223 (2008) 628.
[8] M.J. Evans, V.F. Kranak, Y. Wu, N. Newman, A. Reller, F.J. Garcia-Garcia, U. Häussermann, submitted for publication.
[9] [a] M. Imai, E. Abe, J. Ye, K. Nishida, T. Kimura, K. Homa, H. Abe, H. Kitazawa, Phys. Rev. Lett. 87 (2001) 077003;
[b] M. Imai, K. Nishida, T. Kimura, H. Abe, Appl. Phys. Lett. 80 (2002) 1019.
[10] M. Giantomassi, L. Boeri, G.B. Bachelet, Phys. Rev. B 72 (2005) 224512.
[11] [a] A.D. Taylor, E.J. Wood, J.A. Goldstone, J. Eckert, Nucl. Instrum. Methods Phys. Res. 221 (1994) 408;
[b] F. Mezei, P. Vorderwisch, Physica B 156,157 (1989) 678;
[c] E.I. Litvinenko, E.P. Zhidkov, Comput. Phys. Commun. 127 (2000) 229.
[12] D.S. Sivia, Data Analysis—A Bayesian Tutorial, Oxford University Press, Oxford, 1996.
[13] [a] G. Kresse, J. Furthmüller, Phys. Rev. B 54 (1996) 11169;
[b] G. Kresse, J. Furthmüller, J. Comput. Mater. Sci. 6 (1996) 15;
[c] G. Kresse, J. Hafner, Phys. Rev. B 47 (1993) 558.
[14] J.P. Perdew, Y. Wang, Phys. Rev. B 45 (1992) 13244.
[15] D. Vanderbilt, Phys. Rev. B 41 (1990) 7892.
[16] H.J. Monkhorst, J.D. Pack, Phys. Rev. B 13 (1976) 5188.
[17] [a] K. Parlinski, Z.-Q. Li, Y. Kawazoe, Phys. Rev. Lett. 78 (1997) 4063;
[b] K. Parlinski, Z.-Q. Li, Y. Kawazoe, Phys. Rev. Lett. 81 (1998) 3298.
[18] P.C.H. Mitchell, S.F. Parker, A.J. Ramirez-Cuesta, J. Tomkinson, Vibrational Spectroscopy with Neutrons—With Applications in Chemistry, Biology, Materials Science and Catalysis, in: Series on Neutron Techniques and Applications, vol. 3, World Scientific, Hackensack, NJ, 2005.
[19] [a] A.J. Ramirez-Cuesta, Comput. Phys. Commun. 157 (2004) 226;
[b] D. Champion, J. Tomkinson, G. Kearley, Appl. Phys. A 74 (2002) S1302.
[20] [a] J.-J. Dong, O.F. Sankey, J. Phys. Condens. Matter 11 (1999) 6129;
[b] J.-J. Dong, O.F. Sankey, J. Appl. Phys. 87 (2000) 958;
[c] G.S. Nolas, C.A. Kendziora, J. Gryko, J. Dong, C. Myles, A. Poddar, O.F. Sankey, J. Appl. Phys. 92 (2002) 7225.
[21] S. Aldridge, A.J. Downs, Chem. Rev. 101 (2001) 3305.
[22] A.V. Irodova, V.A. Somenkov, Si.I. Bakum, S.F. Kuznetsova, Z. Phys. Chem. Neue Folge 163 (1989) 239.
[23] N.E. Brese, M. O'Keeffe, R.B. von Dreele, J. Solid State Chem. 88 (1990) 571.
[24] W. Bronger, C.S. Chi, P. Mueller, Z. Anorg. Allg. Chem. 545 (1987) 69.
[25] X. Wang, L. Andrews, J. Phys. Chem. A 107 (2003) 11371.
[26] J. Menéndez, Raman Scattering in Materials Science, in: W.H. Weber, R. Merlin (Eds.), Springer Series in Materials Science, vol. 42, Springer, Berlin, 2000, p. 57.
[27] M.H. Lee, M.J. Evans, L.L. Daemen, O.F. Sankey, U. Häussermann, Inorg. Chem. 47 (2008) 1496.